Published OnlineFirst March 23, 2020; DOI: 10.1158/2326-6066.CIR-19-0467

Enhanced Immunogenicity of Mitochondrial-Localized Proteins in Cancer Cells

Gennaro Prota[1], Uzi Gileadi[1], Margarida Rei[1], Ana Victoria Lechuga-Vieco[1,2,3], Ji-Li Chen[1], Silvia Galiani[1], Melissa Bedard[1], Vivian Wing Chong Lau[1], Lorenzo F. Fanchi[4], Mara Artibani[5,6], Zhiyuan Hu[5,6], Siamon Gordon[7,8], Jan Rehwinkel[1], Jose A. Enríquez[2,9], Ahmed A. Ahmed[5,6], Ton N. Schumacher[4], and Vincenzo Cerundolo[1,†]

ABSTRACT

Epitopes derived from mutated cancer proteins elicit strong antitumor T-cell responses that correlate with clinical efficacy in a proportion of patients. However, it remains unclear whether the subcellular localization of mutated proteins influences the efficiency of T-cell priming. To address this question, we compared the immunogenicity of NY-ESO-1 and OVA localized either in the cytosol or in mitochondria. We showed that tumors expressing mitochondrial-localized NY-ESO-1 and OVA proteins elicit significantdly higher frequencies of antigen-specific $CD8^+$ T cells *in vivo*. We also demonstrated that this stronger immune response is dependent on the mitochondrial location of the antigenic proteins, which contributes to their higher steady-state amount, compared with cytosolic localized proteins. Consistent with these findings, we showed that injection of mitochondria purified from B16 melanoma cells can protect mice from a challenge with B16 cells, but not with irrelevant tumors. Finally, we extended these findings to cancer patients by demonstrating the presence of T-cell responses specific for mutated mitochondrial-localized proteins. These findings highlight the utility of prioritizing epitopes derived from mitochondrial-localized mutated proteins as targets for cancer vaccination strategies.

Introduction

T-cell responses against human cancers contribute to the control of tumor growth, and targeting of CTLA-4 and the PD-1/PD-L1 axis has been very effective in enhancing antitumor immune responses, resulting in clinical objective responses (1, 2), particularly in patients with tumors expressing high mutational burden (TMB; refs. 1, 2). These results underscore an unmet clinical need for many cancer patients with low TMB (i.e., the largest proportion of cancer patients), who could receive greater benefit from immune-checkpoint inhibition treatment, should optimal neoepitopes be identified and used in vaccination strategies.

To this end, new strategies need to be developed to identify the most immunogenic cancer-associated neoepitopes and optimal vaccine platforms to improve immune responses to such predicted epitopes. Current pipelines used for neoantigen prediction have resulted in a low rate of validation, suggesting that the determinants of peptide immunogenicity are still suboptimal (3–5). A greater understanding of the biology of the presentation of the cancer mutanome is thus needed in order to improve such algorithms. Several parameters are currently considered when ranking the immunogenicity of mutations in cancer cells (6–8), but it remains unclear whether the subcellular localization of tumor antigens can modulate the efficiency of priming of antitumor-specific immune responses and whether such parameter should be considered in algorithms ranking immunogenicity of mutated peptides in cancer cells. This represents a critical knowledge gap, as current prognostic scores for responsiveness to immune-checkpoint inhibitors are based mainly on the numbers of mutations, without taking into account whether the subcellular localization of such mutated protein antigens may influence their ability to stimulate an immune response.

Tumor cells fail to directly prime specific immune responses, likely as a result of low costimulation; instead, DCs function simultaneously as both antigen-presenting cells, capable of taking up tumor debris, and IL12-producing cells, in a process referred to as "crosspriming" (9, 10). Evidence that DCs could cross-prime tumor-specific T-cell responses includes the transfer of cellular components from tumor cells to antigen-presenting cells (9, 11). The transfer of mitochondria from tumors to DCs via cytoplasts (11) suggests that mutations in mitochondrial-localized proteins in cancer cells could elicit specific T-cell responses *in vivo*. Consistent with this possibility, activation of the cGAS–STING pathway in DCs may be driven by tumor mitochondrial DNA, resulting in the induction of a type I IFN response (12). Together, these results suggest that tumor-derived mitochondria and mitochondrial-associated antigens play a role in the generation of tumor-specific immune responses.

Previous studies have described the effect of subcellular localization of protein antigens on direct presentation of T-cell epitopes (13–16).

[1]MRC Human Immunology Unit, Weatherall Institute of Molecular Medicine, University of Oxford, Oxford, United Kingdom. [2]Centro Nacional de Investigaciones Cardiovasculares Carlos III, Madrid, Spain. [3]Ciber de Enfermedades Respiratorias (CIBERES), Madrid, Spain. [4]Division of Molecular Oncology and Immunology, Oncode Institute, The Netherlands Cancer Institute, Amsterdam, the Netherlands. [5]Ovarian Cancer Cell Laboratory, Weatherall Institute of Molecular Medicine, University of Oxford, Oxford, United Kingdom. [6]Nuffield Department of Women's and Reproductive Health, University of Oxford, Women's Centre, John Radcliffe Hospital, United Kingdom. [7]Sir William Dunn School of Pathology, University of Oxford, Oxford, United Kingdom. [8]Chang Gung University, Graduate Institute of Biomedical Sciences, College of Medicine, Taoyuan City, Taiwan. [9]Ciber de Fragilidad y Envejecimiento Saludable (CIBERFES), Madrid, Spain.

Note: Supplementary data for this article are available at Cancer Immunology Research Online (http://cancerimmunolres.aacrjournals.org/).

G. Prota and U. Gileadi contributed equally to this article.

†Deceased.

Corresponding Author: Gennaro Prota, WIMM, University of Oxford, Oxford OX3 9DS, UK. Phone: 44-1865-221609; E-mail: gennaro.prota@rdm.ox.ac.uk

Cancer Immunol Res 2020;8:685–97

doi: 10.1158/2326-6066.CIR-19-0467

Published OnlineFirst March 23, 2020; DOI: 10.1158/2326-6066.CIR-19-0467

Yamazaki and colleagues have demonstrated that cytoplasmic versus mitochondrial localization of antigenic protein LIVAT-BP determines which portions of the protein are selected as antigenic epitopes for $CD8^+$ T-cell recognition (16). Although these results are of interest, this paper falls short of distinguishing whether antigen location modulates: (i) *in vivo* cross-priming of T-cell responses; (ii) proteasome-dependent degradation of the antigenic protein; and (iii) tumor growth.

Here, we have investigated both *in vitro* and *in vivo* the impact of the mitochondrial location of antigenic proteins on direct- and cross-priming, as compared with the immunogencity of the same antigenic proteins expressed in the cytosol. We have extended results obtained in animal models to clinical samples by demonstrating the presence of $CD8^+$ T-cell responses specific to mitochondrial-localized neoantigens in a patient with endometrial cancer. Our results demonstrate that mitochondrial-localized proteins induce greater immune responses than cytosol-localized proteins and provide a rationale for including protein localization data to improve prediction algorithms for neoepitopes that are effective in priming immune responses.

Materials and Methods

Mice

STING knockout (17), cGAS knockout (18), MAVS knockout (19), Myd88 knockout, MARCO/SRA knockout, β_2-microglobulin knockout, human leukocyte antigen (HLA)-A2.1 transgenic mice (HHD mice; ref. 20), and C57BL/6 control mice were bred in the local animal facility under specific pathogen–free conditions and used at 6 to 10 weeks of age. Mice were injected subcutaneously (s.c.) with 1×10^6 or 10^5 cells/mouse for immunogenicity or tumor growth experiments, respectively. Animal studies have been conducted in accordance with, and with the approval of, the United Kingdom Home Office. All procedures were done under the authority of the appropriate personal and project licenses issued by the United Kingdom Home Office License number PBA43A2E4.

Cloning and cell lines

A cDNA fragment containing sequences encoding amino acids 1–22 of the human arginase-2 protein followed by OVA amino acids 47–386 (or NY-ESO-1) and the HA tag (YPYDVPDYA) was synthetically made by Thermo Fisher Scientific. This was inserted into plasmid pHR-SIN-MCS-ires-eGFP (5) to create pLenti-mtOva or pLenti mtNY-ESO-1. Using PCR, $OVA_{47\text{-}386}$HA (or NY-ESO-1-HA) lacking the mitochondrial directing sequence were generated to create pLenti-cytoOVA or pLenti cytoNY-ESO-1 (in pHR-SIN-MCS-ires-eGFP). Using PCR, additional primers allowed us to add other sequences to the N-terminus of $OVA_{47\text{-}386}$. One such construct, although initially intended to direct OVA to the nucleus (by addition of an N-terminal MPKKKRVGG sequence), failed to do so and instead was shown experimentally, to produce a cytoplasmically located, yet more stable OVA protein. B16 cells transfected with this construct were named B16 mod cytoOVA. A fusion with an N-terminal mCherry protein was generated by inserting the mitochondria targeted $OVA_{47\text{-}386}$ gene into the plasmid pHR-SIN mCherry (21). The plasmids described above were used to produce lentiviral particles that were then used to transduce CT26 cells, B16F10 cells, and Lewis lung carcinoma cells (LLC). Cells were used between passages 4 and 8 and routinely tested for *Mycoplasma* contamination. The LLC cell line has been received from the ATCC in 2019, B16F10 was kindly provided by Dr. Michael Palmowsky (University of Oxford, NDM) in 2002, and CT26 from Dr. Jonathan Silk (Adaptimmune) in 2012. The cell lines were not authenticated in the past year.

Western blot

Whole-cell lysates or subcellular fractions were boiled in sample buffer, separated using SDS/PAGE, transferred to PVDF membranes (Bio-Rad), and blocked with 5% (weight/vol) skimmed milk in 0.5% Tween 20 in TBS for 1 hour at room temperature. Membranes were probed using anti OVA, anti-GAPDH, anti-TOM20, anti-NY-ESO-1, anti-ATPβ, and HRP-conjugated rat anti-mouse or donkey anti-rabbit according to the primary antibody used. Antibody clones are reported in Supplementary Table S1. HRP reaction was developed using Supersignal West Pico kit (Thermo Fisher Scientific).

Confocal microscopy

Cells were stained with Mitotracker Red CMX-Ros (50 nmol/L 15 minutes at 37°C; Thermo Fisher Scientific) and fixed with 3% formaldehyde in PBS (Thermo Fisher Scientific), permeabilized for 15 minutes with PBS Triton-X (Sigma-Aldrich) 1%, and blocked with 2% serum bovine albumin (BSA; Sigma-Aldrich) + 5% fetal calf serum (FCS, Sigma-Aldrich) in PBS for 1 hour at room temperature. Samples were incubated with primary antibodies in blocking buffer for 1 hour at room temperature. After several washing steps, the cells were incubated for 30 minutes with secondary antibodies conjugated to Abberior STAR 600 and/or Abberior STAR Red (Abberior Instruments) diluted 1:250 in 1% BSA in PBS. After several washing steps, the slides were mounted on a drop of Mowiol (Sigma-Aldrich). A pixel-wise Pearson colocalization test to quantify the colocalization of mitotracker and NY-ESO-1 was performed (values of 1 indicate complete colocalization, 0 indicates no colocalization).

In vitro and *ex vivo* staining of B16 cell lines

B16 cytoOVA, B16 mtOVA, and B16 wild-type (WT) cells were incubated with IFNγ, TNFα, or both (5 ng/mL; BioLegend) for 2 or 5 days and then stained with the H-$2K^b$-$OVA_{257\text{-}264}$–specific antibody (22). Stimulated cells were cocultured with OT-I $CD8^+$ T cells (ratio 1:40) overnight, and OT-I cells were stained for extracellular markers (CD8α, CD69, and CD25) and viability (antibody clones are reported in Supplementary Table S2). C57BL/6 mice were injected with B16 mtOVA or B16 cytoOVA and B16 WT. Tumors were collected, pierced, and minced in 24-well plates and incubated for 15 minutes at 37°C in 1 mL of digestion buffer (2 mg/mL collagenase D, and 1 mg/mL DNAse I in RPMI-1640, both from Sigma-Aldrich). After the first 15 minutes of incubation, cells were pipetted up and down repeatedly, then returned for a second 15-minute incubation at 37°C. After digestion, B16 cells were stained with H-$2K^b$-$OVA_{257\text{-}264}$– and CD105-specific antibodies. Samples were acquired on a FACScanto II (BD Biosciences) flow cytometer, and data were analyzed with FlowJo version 10.4.1. Compensation beads (eBioscience) were used to generate the compensation matrix, and fluorescence minus one (FMO) were used as control.

Ex vivo peptide restimulation assay and intracellular staining

Splenocytes (2×10^6) were isolated from either naïve or tumor-bearing C57BL/6 mice 7 days after the injection and were cultured in the presence of $OVA_{257\text{-}264}$ peptide (SIINFEKL; Sigma-Aldrich) or NY-ESO-$1_{157\text{–}165}$ peptide (SLLMWITQC, Sigma-Aldrich) peptide in complete RPMI-1640 medium supplemented with 10% FBS, 2.1 mmol/L ultra-glutamine in the presence of Brefeldin A (5 μg/ml) and monensin (2 μM; BioLegend). After 5 hours of incubation, cells were stained for extracellular markers (CD8b, B220, CD44, CD69,

Published OnlineFirst March 23, 2020; DOI: 10.1158/2326-6066.CIR-19-0467

and CD25) and viability (antibody clones are reported in Supplementary Table S2). Cells were then stained for intracellular IFNγ and TNFα using an Intracellular Fixation and Permeabilization Buffer Set (eBioscience) according to the manufacturer's instructions. Samples were acquired on a FACScanto II (BD Biosciences) flow cytometer, and data were analyzed with FlowJo version 10.4.1. Compensation beads (eBioscience) were used to generate the compensation matrix, and FMOs were used as control.

Depletion of CD8$^+$ T cells

Mice were injected on days 0 and 2 with 400 μg/mouse of CD8 antibody intraperitoneally (anti-CD8 clone 2.43 or isotype control, both from Invivomab). On day 2, mice were injected with the B16 tumor cells s.c. (1.5×10^5 cells/mouse) and were then injected every 6 days with 200 μg/mouse of CD8 antibody intraperitoneally. To confirm the depletion of CD8$^+$ T cells, blood samples were collected from the tail on days 6 and 10 in tubes with heparin. Red blood cells were lysed with red blood cells lysis buffer (Qiagen) following the manufacturer's instruction. After washing, cells were stained for extracellular markers (CD8b, CD3, and B220) and viability (antibody clones are reported in Supplementary Table S2). The same staining was performed on splenocytes on day 14, after which the mice were killed. Samples were acquired on a FACScanto II (BD Biosciences) flow cytometer, and data were analyzed with FlowJo version 10.4.1. Compensation beads (eBioscience) were used to generate the compensation matrix and FMOs were used as control.

Vaccination of mice with isolated mitochondria

Mitochondria from B16 tumor cells or from mouse adult fibroblasts were isolated as previously described (23). Mice were injected with 50 μg of the mitochondrial protein samples. On day 10 after vaccination, mice were challenged with B16 or LLC tumor cell lines and the tumor growth was monitored. Where indicated, CD8$^+$ T cells were depleted before tumor injection. CD8$^+$ T-cell responses were evaluated 14 days after tumor injection: CD8$^+$ T cells were isolated from mice spleens with a CD8 isolation kit (Miltenyi Biotech) and cocultured overnight with B16 cells that had been previously stimulated 48 hours with IFNγ (10 ng/mL). Brefeldin A and monensin were added for the last 5 hours of coculture. Cells were then stained for extracellular markers (CD8b, B220, and CD44) and viability (antibody clones are reported in Supplementary Table S2). Cells were then stained for intracellular IFNγ using an Intracellular Fixation and Permeabilization Buffer Set (eBioscience) according to the manufacturer's instructions. Samples were acquired on a FACScanto II (BD Biosciences) flow cytometer, and data were analyzed with FlowJo version 10.4.1. Compensation beads (eBioscience) were used to generate the compensation matrix and FMOs were used as control.

Pan-cancer analysis of somatic mutations

The somatic mutation data were downloaded from The Cancer Genome Atlas (TCGA) Genomic Data Commons data portal (https://portal.gdc.cancer.gov). The somatic mutation data (version 02-04-2018) included 9,508 samples from 31 cancer types (Supplementary Table S3). The somatic mutations were generated by MuTect2 (24) with the GRCh38 reference genome. To calculate the number of nonsilent somatic mutations locating in mitochondrial genes, we kept the somatic mutations that passed the filter of the mutation calling, located in the genes that belong to Gene Ontology GO:0005739 (cellular component: mitochondrion) and were classified as nonsilent mutations. We used the in-house R script to filter mutations and perform visualization. The R code is available at https://github.com/zhiyhu/mito-mut-pancan.

Neoantigen prediction and selection of peptides for screening

Endometrial tumor tissue and blood collection were obtained from a patient recruited to the Gynecological Oncology Targeted Therapy Study 01 (GO-Target-01) under research ethics approval number 11-SC-0014, good clinical practice based on the Declaration of Helsinki were used. The patient gave informed consent. Whole-genome sequencing was performed on blood and tumor tissues (BGI Tech Solutions Ltd) as previously described (25). RNA was extracted using the Qiagen RNeasy Mini Kit, and its quality was assessed with the Agilent TapeStation before preparing the sequencing libraries. Two technical replicates were prepared from 400 ng RNA, each using the NEBNext Ultra Directional RNA Library Prep Kit for Illumina (E7420) in combination with the NEBNext Poly(A) mRNA Magnetic Isolation Module (E7490) and NEBNext Q5 Hot Start HiFi PCR Master Mix (M0543). The libraries were indexed and enriched by 14 cycles of amplification, assessed using the Agilent TapeStation and then quantified by Qubit. Multiplexed library pools were quantified with the KAPA Library Quantification Kit (KK4835) and sequenced using 80 bp PE reads on the Illumina NextSeq500 platform. Tumor-specific nonsynonymous mutations were predicted and ranked as previously shown (26). Peptides were synthesized by Pepscan Presto BV.

Expansion of antigen-specific T cells

One hundred twenty peptides were pooled in 6 groups of 20 peptides each. *In vitro* stimulation of CD8 T cells was done as previously described (27). Briefly, 5×10^6 to 8×10^6 peripheral blood mononuclear cells (PBMC) from the patient were stimulated with each peptide pool at a final concentration of 20 μg/mL (2 μg/mL, each peptide) for 3 days in RH10 [RPMI with 10% heat-inactivated human serum (Sigma), 2 mmol/L L-glutamine, 10 mmol/L HEPES, 1 mmol/L sodium pyruvate, nonessential amino acids (1×), penicillin (25,000 U), streptomycin (25 mg), 50 μmol/L β-mercaptoethanol (Gibco)] supplemented with 25 ng/mL human IL7 (PeproTech). On day 3, half of the media were replaced with RH10-IL2 (RH10 supplemented with 1,000 IU human IL2; Novartis). When confluent, cells were split using RH10-IL2. To further increase cell expansion, 4 weeks later, cells were restimulated with phytohaemagglutinin 1 μg/mL in RH10-IL2 and in the presence of irradiated PBMC feeders and rest for 3 to 4 weeks before screening.

Neoantigen-specific T-cell screening

Generation of peptide–MHC class I monomers and tetramerization was performed as previously described (28). Briefly, biotin-tagged HLA-A2 complexes were folded with the UV-sensitive peptide KILGFVFJV. Two micrograms of HLA-A2 complexes was UV exchanged for 1 hour with each screening peptide at a final concentration of 200 μg/mL, in 20 μL. After centrifugation at $2{,}250 \times g$, 1.5 μg of complexes (15 μL supernatant) was collected and tetramerized with 1.5 μL of a 1:1 mix streptavidin-APC/streptavidin-PE (eBioscience). Free biotin in the complexes was blocked by adding 20 μL of 50 μmol/L D-biotin. Stimulated PBMCs (1×10^5) were incubated in 50 μL staining buffer (PBS 0.5% BSA) containing 2.5 μL of multimers, for 30 minutes at 37°C. Cells were washed two times with staining buffer and stained with LIVE/DEAD Fixable Aqua (Thermo Fisher Scientific), anti-CD3 FITC (clone SK7, BioLegend), and anti-CD8 PerCP-Cy5.5 (clone SK1,

Published OnlineFirst March 23, 2020; DOI: 10.1158/2326-6066.CIR-19-0467

BioLegend). Cells were analyzed in a BD LSRFortessa instrument. PE and APC tetramer-positive cells were sorted in a BD fusion instrument and further expanded for functional assays.

VITAL assay

Autologous Epstein–Barr virus-transformed lymphoblastoid cell lines (EBV-LCL) were generated from PBMCs, using supernatant of EBV producing B95-8 marmoset cells and 2 μg/mL cyclosporin A (Sigma). EBV-LCLs used as target cells were loaded with 1 μmol/L peptides, for 1 hour at 37°C. Loaded and nonloaded cells were stained with either CellTrace Far Red or CellTracker Orange CMTMR dyes (Thermo Fisher Scientific) and quenched with FCS. After two wash cycles, loaded and nonloaded targets were mixed in a 1:1 ratio and plated in a 96 U-bottom well plate. Effector T cells, previously incubated overnight in the absence of IL2, were added to the wells at the indicated effector-to-target ratio, in duplicates. Following 4.30 hours of incubation at 37°C, cells were stained with LIVE/DEAD Fixable Aqua (Thermo Fisher) and anti-CD8-FITC (clone SK1, BioLegend). Cells were analyzed in a BD LSRFortessa instrument.

ELISA

EBV-LCLs were loaded with 1 μmol/L peptide, for 1 hour at 37°C, and washed twice. Loaded cells were plated at 25,000 cells per well in a U-bottom 96-well plate and used to stimulate 2,500 T cells, in duplicates. Following 16 hours of incubation, the production of IFNγ was assessed by ELISA (BD Pharmingen).

Results

Targeting to mitochondria enhances cross-priming of protein-specific CD8$^+$ T cells

To investigate whether mitochondrial proteins contained within tumor cells could be transferred to antigen-presenting cells (APC) during tumor growth *in vivo*, B16 cells were transduced with lentiviral vectors encoding mitochondrial-localized ovalbumin (OVA) fused with the fluorescent protein mCherry (B16 mtOVA-mCherry), which were then injected subcutaneously in mice. The results of these experiments showed that CD103$^+$ and CD11b$^+$ migratory DCs had preferentially taken up mCherry protein, compared with CD8α$^+$ DCs, CD169$^+$ macrophages, and CD11b$^+$ resident DCs (Supplementary Fig. S1A). In addition, the uptake of mitochondrial-localized mtOVA-mCherry correlated with enhanced DC maturation, as shown by higher CD86 expression on mtOVA-mCherry$^+$ DCs cells compared with mtOVA-mCherry$^-$ DCs (Supplementary Fig. S1B and S1C).

The uptake of mitochondrial-localized ovalbumin-mCherry fusion protein by migratory DCs suggested that the phagocytosis of mitochondria by CD103$^+$ DCs may elicit the cross-priming of T cells specific for antigenic mitochondrial proteins. To address this, the H-2^d tumor cell line CT26 was transduced with a lentiviral vector encoding either NY-ESO-1 or OVA proteins, which were either targeted to mitochondria (CT26 mtNY-ESO-1 or CT26 mtOVA) or localized in the cytosol (CT26 cytoNY-ESO-1 or CT26 cytoOVA) and then injected into MHC-mismatched mice to assess their ability to induce cross-priming of antigen-specific CD8$^+$ T cells. Mitochondrial and cytosolic targeting was confirmed by confocal microscopy (**Fig. 1A**; Supplementary Fig. S2A and S2B).

We have previously shown that HLA-A2.1 transgenic mice (HHD mice) can generate HLA-A2–restricted CD8$^+$ T cells upon vaccine injection (20, 29). We therefore challenged HHD mice with the mismatched H-2^d tumor cell line CT26 mtNY-ESO-1 and CT26 cytoNY-ESO-1 and compared the frequency of HLA-A2–restricted NY-ESO-1$_{157\text{-}165}$–specific T cells. Because CT26 cells do not express HLA-A2 molecules, priming of HLA-A2–restricted NY-ESO-1–specific responses is dependent on cross-presentation events controlled by HHD-mice resident HLA-A2$^+$ DCs.

Injection of CT26 mtNY-ESO-1 cells into HLA-A2$^+$ HHD mice resulted in a significantly higher frequency of NY-ESO-1–specific HLA-A2–restricted CD8$^+$ T cells than the injection of CT26 cytoNY-ESO-1 cells. CD8$^+$ T-cell responses were only marginally higher following injection of CT26 cytoNY-ESO-1 cells than in mice injected with WT CT26 cells, as measured by staining with HLA-A2/NY-ESO-1$_{157–165}$ tetramers and intracellular staining for IFNγ and TNFα (**Fig. 1B**; Supplementary Fig. S2C).

These results were confirmed by injecting mismatched CT26 mtOVA cells into C57BL/6 mice, which generated a significantly higher frequency of H-2K^b/SIINFEKL–specific CD8$^+$ T-cell responses compared with the CT26 cytoOVA cell line, independent of the level of expression of the OVA transgene (**Fig. 1C**; Supplementary Fig. S2E–S2G). CT26 mtOVA was also superior to CT26 cytoOVA at inducing H-2K^b/SIINFEKL–specific CD8$^+$ T-cell responses, as measured by induction of proliferation of adoptively transferred OT-I CD8$^+$ T cells (Supplementary Fig. S2H).

These findings demonstrate that the cross-priming of CD8$^+$ T cells specific for NY-ESO-1 and OVA proteins, in HHD and B6 mice, respectively, is enhanced by the targeting of these antigens to mitochondria.

We next analyzed the steady-state amount of NY-ESO-1 and OVA proteins and their stability in the presence or absence of proteasome inhibitors (**Fig. 1D**; Supplementary Fig. S2I). The steady-state amount of mitochondrial-localized NY-ESO-1 (**Fig. 1D**) and OVA (Supplementary Fig. S2I) proteins was preserved in the absence of proteasome inhibitors, compared with cytosolic NY-ESO-1 or OVA proteins, which appear to be degraded in the absence of proteasome inhibitors.

In conclusion, relocation of NY-ESO-1 and OVA proteins from the cytosol to mitochondria increases their stability and steady-state amount, resulting from protection from proteasome degradation, and hence, enhancing their ability to be cross-presented *in vivo*.

Enhanced immunogenicity of mitochondrially localized OVA in syngeneic mice

We next assessed whether the enhanced immunogenicity of mitochondrial-localized NY-ESO-1 and OVA proteins could be confirmed in a syngeneic mouse model. B16 melanoma cells were transduced with lentiviral vectors encoding either mitochondrial-targeted OVA (B16 mtOVA) or cytosolic OVA (B16 cytoOVA). In both cell lines, the expression of OVA was linked to the expression of the reporter protein GFP. We observed that cytosolic OVA was rapidly degraded by the proteasome, and that inhibition of proteasome activity with epoxomicin rescued B16 cytoOVA to amounts equivalent to that of B16 mtOVA (**Fig. 2A** and **B**). Consistent with equal protein amounts of OVA in B16 mtOVA and B16 cytoOVA cells, OVA mRNA (Supplementary Fig. S3A) and GFP expression was equivalent (**Fig. 2A**). B16 mtOVA and B16 cytoOVA cells were injected into C57BL/6 mice, and 7 days later, the H-2K^b/SIINFEKL–specific CD8$^+$ T-cell response was measured in the spleen. Consistent with previous results using the mismatched CT26 cell lines, B16 mtOVA doubled the frequency of OVA-specific CD8$^+$ T cells compared with B16 cytoOVA (**Fig. 2C**).

In order to assess whether the enhanced priming of the OVA response upon injection of B16 mtOVA cells was due solely to OVA's increased stability or if the location of OVA in mitochondria had an additional role accounting for its enhanced priming ability, we

Published OnlineFirst March 23, 2020; DOI: 10.1158/2326-6066.CIR-19-0467

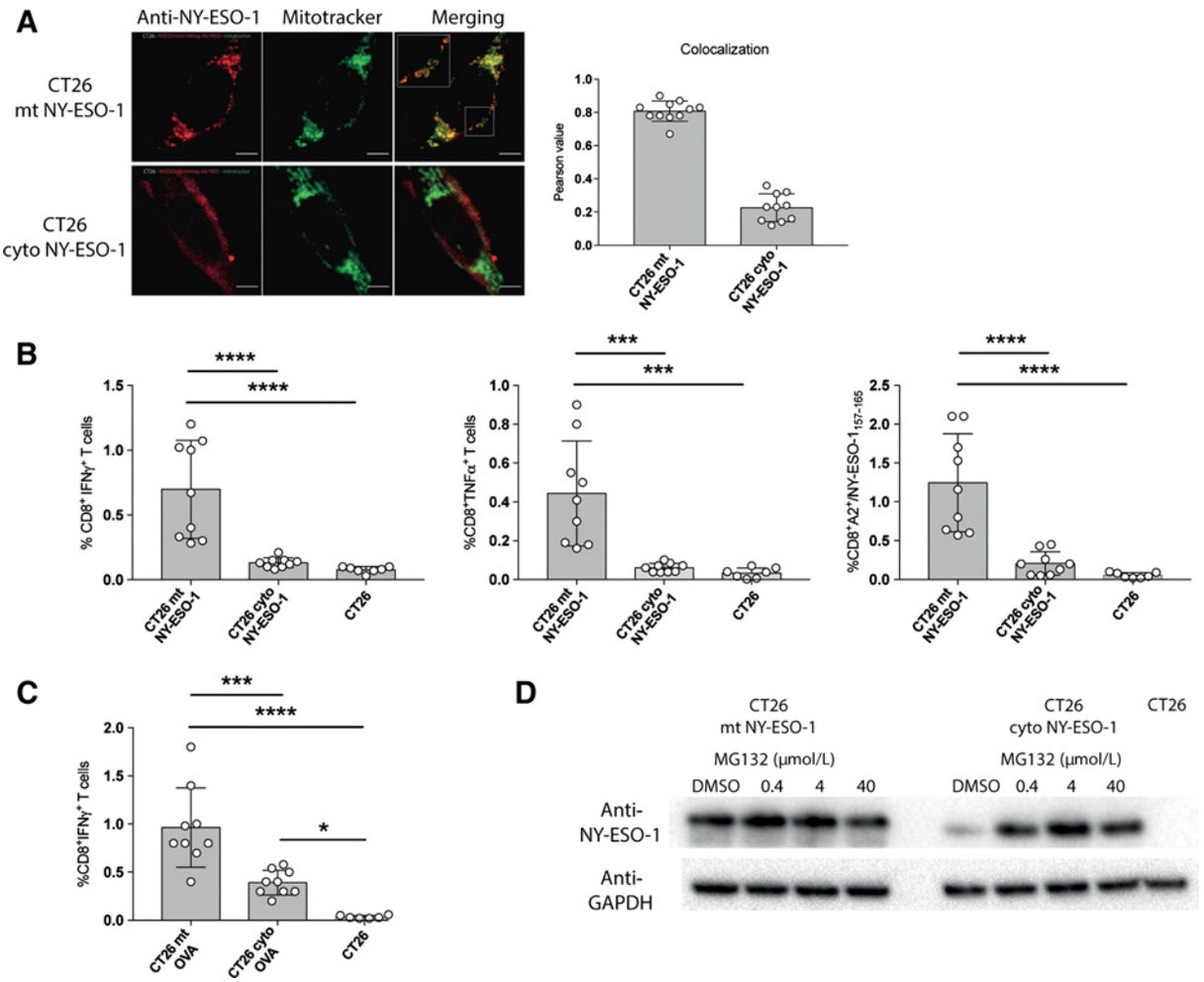

Figure 1.

Cross-priming of CD8$^+$ T cells specific for OVA or NY-ESO-1 is enhanced by their targeting to mitochondria. **A,** Representative dual-color confocal images of CT26 cells stably expressing NY-ESO-1 localized in the cytosol (CT26 cytoNY-ESO-1, bottom) or in the mitochondria (CT26 mtNY-ESO-1, top) with the mitochondrial dye mitotracker (green) and immunostaining (red) for NY-ESO-1. A pixel-wise Pearson colocalization test to quantify the colocalization of mitotracker and NY-ESO-1 localization is shown on the right. Results are representative of two independent experiments. **B,** HHD mice ($n = 5$ per group) were injected with 1×10^6 CT26 mtNY-ESO-1, cytoNY-ESO-1, or WT cells. Seven days after the injection, splenocytes were stained with HLA-A2 NY-ESO-$1_{157–165}$ tetramers (right) or restimulated with the NY-ESO-$1_{157–165}$ peptide (SLLMWITQC), and production of IFNγ (left) and TNFα (middle) was assessed by intracellular staining. Data are representative of at least two independent experiments; values are expressed as mean ± SD. **C,** C57BL/6 mice ($n = 5$ per group) were injected with 2×10^6 CT26 mtOVA, cytoOVA, or WT cells. Seven days after the injections, splenocytes were restimulated with the OVA peptide (SIINFEKL) for 5 hours, and the production of IFNγ was assessed by intracellular staining. Data are representative of at least two independent experiments with $n = 5$, and values are expressed as mean ± SD. **D,** CT26 mtNY-ESO-1 and cytoNY-ESO-1 tumor cell lines were cultured in the presence of the proteasome inhibitor MG132 at the indicated concentrations or DMSO for 3 hours. Western blotting was performed with indicated antibodies. **B** and **C,** ****, $P < 0.0001$; ***, $P < 0.001$; *, $P < 0.05$ (one-way ANOVA followed by Tukey posttest).

generated a modified cytosolic OVA (hereafter referred to as "mod cytoOVA") with an N-terminal extension of 9 amino acids. When mod cytoOVA was expressed in B16 cells, it resulted in a significantly higher steady-state amount of OVA compared with WT cytosolic and mitochondrial OVA (**Fig. 2A**) and was less sensitive to proteasomal degradation (**Fig. 2A**). Fractionation of B16 mod cytoOVA cell lysates confirmed the enrichment of mod cytoOVA protein in the cytosolic fraction and not mitochondrial, as reference proteins for mitochondrial-localized or cytosolic localized protein TOM20 (the mitochondrial outer membrane translocase) and GAPDH (glyceraldehyde 3-phosphate dehydrogenase) were used, respectively (**Fig. 2B**). Consistent with the notion that the steady-state amount of antigenic proteins determines the potency of their immunogenicity *in vivo* (13, 30, 31), we observed that the frequency of OVA-specific CD8$^+$ T-cell response following the injection of B16 mod cytoOVA was significantly greater than in B6 mice injected with B16 cytoOVA. However, despite the greater amount of steady-state OVA in B16 mod cytoOVA cells, priming of the OVA-specific CD8$^+$ T-cell response in mice injected with B16 mtOVA was more efficient than in mice primed with B16 mod cytoOVA cells (**Fig. 2C**), suggesting that the localization of OVA into mitochondria confers a distinct priming advantage in addition to its increased steady-state amount.

Published OnlineFirst March 23, 2020; DOI: 10.1158/2326-6066.CIR-19-0467

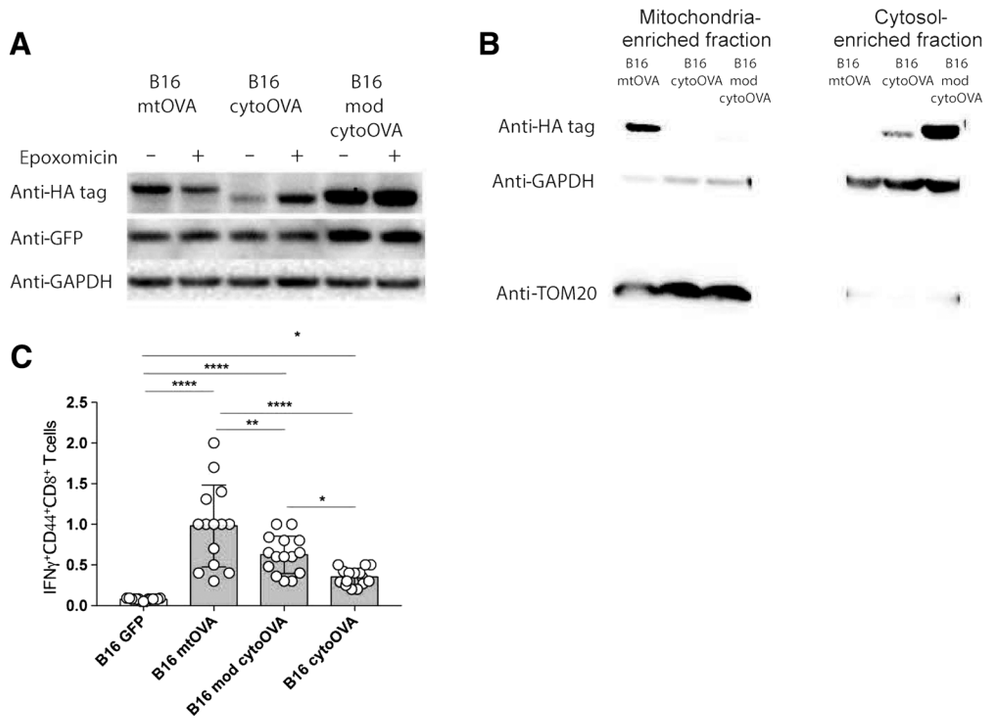

Figure 2.

Mitochondrial-localized OVA primes higher frequency of $CD8^+$ T-cell responses *in vivo* as compared with cytosolic-localized OVA. **A,** B16 mtOVA, cytoOVA, and mod cytoOVA cells were cultured in the presence of the proteasome inhibitor epoxomicin (0.2 μmol/L) or DMSO for 3 hours. Western blotting was performed with indicated antibodies. **B,** The localization of OVA in different compartments was demonstrated by Western blot of different cellular fractions. **C,** C57BL/6 mice were injected with 1×10^6 B16 mtOVA, cytoOVA, mod cytoOVA, or control cells. Seven days after the injection, splenocytes were restimulated with the $OVA_{257–264}$ peptide, and the production of IFNγ was assessed by intracellular staining. Bars represent the mean frequencies ± SD of 14 mice from two independent experiments. ****, $P < 0.0001$; **, $P < 0.01$; *, $P < 0.05$ (one-way ANOVA followed by Tukey posttest).

Superior T cell–priming ability of mtOVA cells results in enhanced tumor control

It is established that the rate of degradation of antigenic proteins directly correlates with the generation of MHC class I epitopes presented on the surface of APCs (32, 33). Consistent with this notion, the reduced stability of OVA in B16 cytoOVA was associated with a greater amount of the H-$2K^b$/SIINFEKL epitope generated by B16 cytoOVA both *in vitro* (**Fig. 3A**) and *ex vivo* (**Fig. 3B**; Supplementary Fig. S4A and S4B), as measured by flow cytometry for H-$2K^b$/SIINFEKL expression (22) and by increased expression of activation markers on OT-I splenoctyes *in vitro*, suggesting T-cell proliferation (**Fig. 3C** and **D**). Direct presentation of the SIINFEKL epitope *in vivo* on the surface of B16 mtOVA cells was detectable only after 14 days from the injection (**Fig. 3B**). Upregulation of H-$2K^b$/SIINFEKL complexes on the surface of B16 cells both *in vitro* and *in vivo* was dependent on cytokine stimulation, and in particular on the combined effect of IFNγ and TNFα (Supplementary Fig. S4C). A statistically significant greater amount of the H-$2K^b$/SIINFEKL complex was also observed on the surface of LLC encoding cytoOVA than on LLC encoding mtOVA *in vitro* (Supplementary Fig. S4D). These results demonstrated that rapid proteasome-dependent degradation of cytoplasmic OVA in B16 cells was very efficient in directly presenting the H-2 K^b/SIINFEKL epitope, which resulted in greater activation of SIINFEKL-specific $CD8^+$ T cells, as compared with mitochondrial-localized OVA and more stable cytosolic OVA in B16 cells.

The findings from the above *in vitro* experiments (**Fig. 3A–D**) combined with the results from the *in vivo* immunogenicity experiments (**Fig. 2C**), together with previously published studies (30–32), show an inverse relationship between efficient direct antigen presentation of tumor cells and their ability to efficiently prime an *in vivo* antigen-specific immune response. Because both of these processes are required to generate an efficient tumor-specific immune response capable of controlling tumor growth, we monitored the rate of B16 growth *in vivo* and demonstrated a slower growth of B16 mtOVA than B16 cytoOVA cells (**Fig. 3E**), which was dependent on the presence of $CD8^+$ T cells (**Fig. 3F**). These findings were further supported by the observation that B16 mtOVA tumors grew unhindered in β-2 microglobulin knockout mice (**Fig. 3G**). As a control, we showed that both tumor cell lines had a similar *in vitro* growth rate (Supplementary Fig. S3B).

In conclusion, these results demonstrate that direct presentation of the H-$2K^b$/SIINFEKL epitope by B16 cells is more efficient in cells expressing cytoplasmic OVA than mitochondrial OVA, but the amount of the directly presented SIINFEKL peptide on the surface of B16 mtOVA *in vivo* is sufficient for optimal tumor control.

The cGAS–STING pathway enhances immunogenicity of B16 mtOVA cells

Previous studies have demonstrated that the efficiency of priming of tumor-specific T-cell responses is enhanced by the release of DNA from tumor cells, which acts as a natural adjuvant to activate the

Published OnlineFirst March 23, 2020; DOI: 10.1158/2326-6066.CIR-19-0467

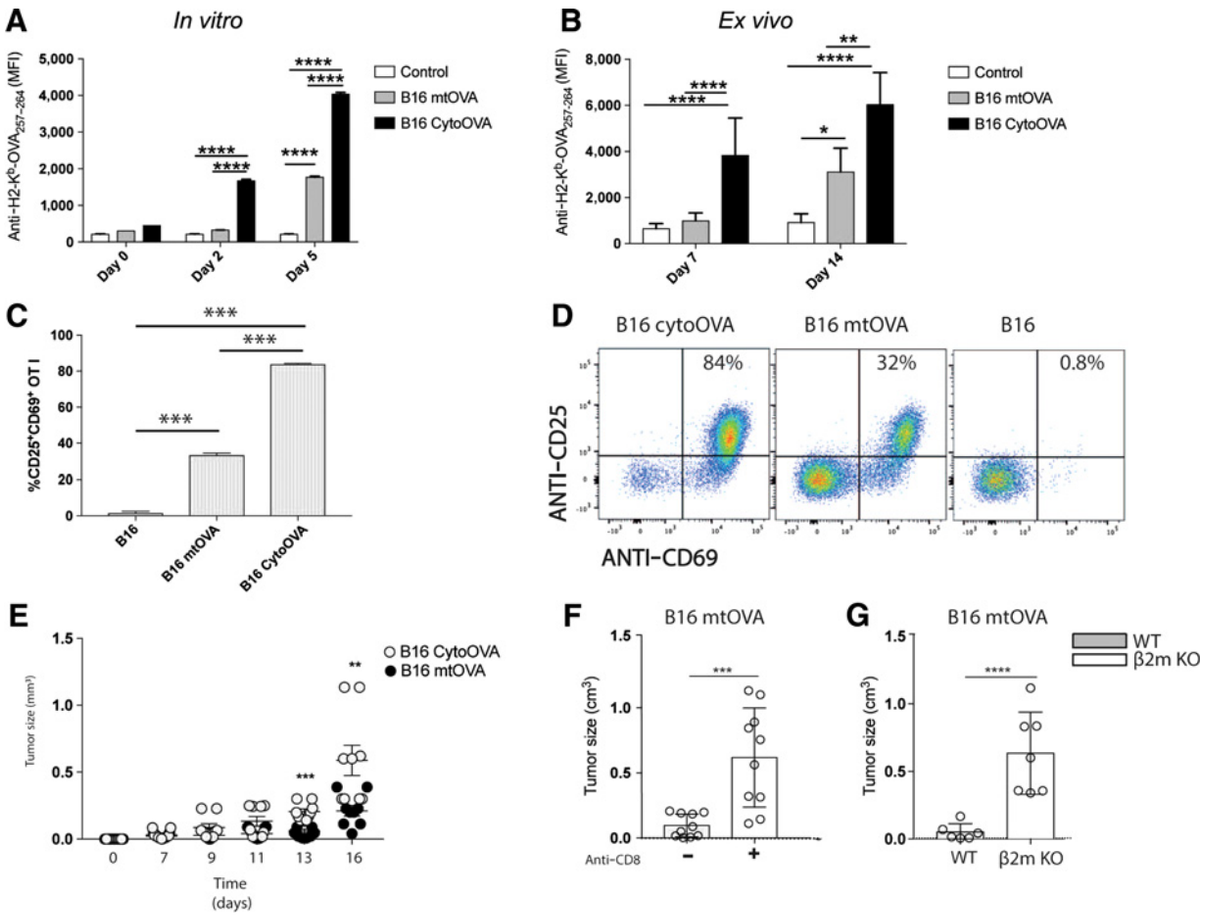

Figure 3.

Subcellular location of OVA modulates the efficiency of its direct presentation to OVA-specific CD8$^+$ T cells. **A,** B16 cytoOVA, mtOVA, and GFP were incubated with IFNγ and TNFα (5 ng/mL) for the indicated number of days and then stained with an H-2K^b-OVA$_{257–264}$ antibody (expressed as MFI). **B,** C57BL/6 mice were injected with B16 mtOVA, cytoOVA, and GFP. Tumor cells were isolated on indicated days and stained with an H-2K^b-OVA$_{257–264}$ antibody; results are shown as MFI. Data are representative of two or three independent experiments with $n = 5$, and values are expressed as mean ± SD. ****, $P < 0.00001$; **, $P < 0.001$; *, $P < 0.01$ (one-way ANOVA followed by Tukey posttest). **C,** B16 cytoOVA, mtOVA, and WT were treated for 5 days with IFNγ and TNFα and then cocultured with OT-I T cells in triplicates. Expression of activation markers on OT-I splenocytes was investigated after 24 hours. **D,** Representative plots are shown. **E,** B16 mtOVA and cytoOVA were injected s.c. in the flank (1.5 × 10^5 cells/mouse); tumor growth curves at different time points are shown**.** Data are representative of two or three independent experiments with $n = 8$, and values are expressed as mean ± SEM. Two-tailed Student *t* test was used for comparing values. ***, $P < 0.001$; **, $P < 0.01$. **F,** Groups of C57BL/6 mice were injected on days 0, 3, and 8 with a CD8 antibody or with an isotype control. On day 3, mice were injected s.c. with B16 mtOVA (1.5 × 10^5 cells/mouse); tumor size on day 16 is shown. Bars represent the mean tumor size ± SD of 10 mice from two independent experiments. Two-tailed Student *t* test was used for comparing values. ****, $P < 0.0001$; ***, $P < 0.001$. **G,** B16 mtOVA cells were injected s.c. in the flank (1.5 × 10^5 cells/mouse) of WT or beta 2 microglobulin knockout (KO) C57BL/6 mice, and tumor size at day 14 is shown. MFI, mean fluorescence intensity.

STING pathway and induce a type I IFN response (34, 35). We assessed the role of STING and cGAS in the enhanced immunogenicity of mtOVA B16 cells. The frequency of H-2K^b/SIINFEKL CD8$^+$ T cells in STING knockout mice injected with B16 mtOVA cells was significantly reduced compared with WT mice (**Fig. 4A**), whereas no differences were observed after the injection of B16 cytoOVA (**Fig. 4B**). Similar results were obtained using cGAS knockout mice (**Fig. 4C**). As a control, vaccination of cGAS and STING knockout mice with adjuvant full-length OVA protein resulted in a similar frequency of H-2K^b/SIINFEKL CD8$^+$ T cells as in WT mice (Supplementary Fig. S5A and S5B). The frequency of OVA-specific IFNγ$^+$ T cells in mice lacking expression of Myd88, NLRP3, or MAVS was similar to those in WT mice injected with B16 mtOVA cells (**Fig. 4D**).

In order to further assess the identity of DCs responsible for the cross-priming of OVA-specific CD8$^+$ T cells, we investigated the immunogenicity of mitochondrial-localized OVA in BATF3 knockout mice, in which the development of CD103$^+$/CD8α cross-presenting DCs is compromised (36). Consistent with our earlier observations demonstrating that mtOVA-mCherry is taken up by CD103$^+$ DCs (Supplementary Fig. S1), injection of B16 mtOVA into BATF3 knockout mice failed to elicit detectable H-2K^b/SIINFEKL–specific CD8$^+$ T-cell responses as compared with the response seen in WT C57BL/6 mice, suggesting a role for cross-presenting DCs (**Fig. 4E**). Next, we sought to identify the receptor involved in the uptake of mtOVA cells. In mice lacking the F-actin receptor DNGR-1 (37) and in double-knockout mice lacking the expression of the collagen scavenger receptor MARCO and the scavenger receptor A (SRA; ref. 38), we

Published OnlineFirst March 23, 2020; DOI: 10.1158/2326-6066.CIR-19-0467

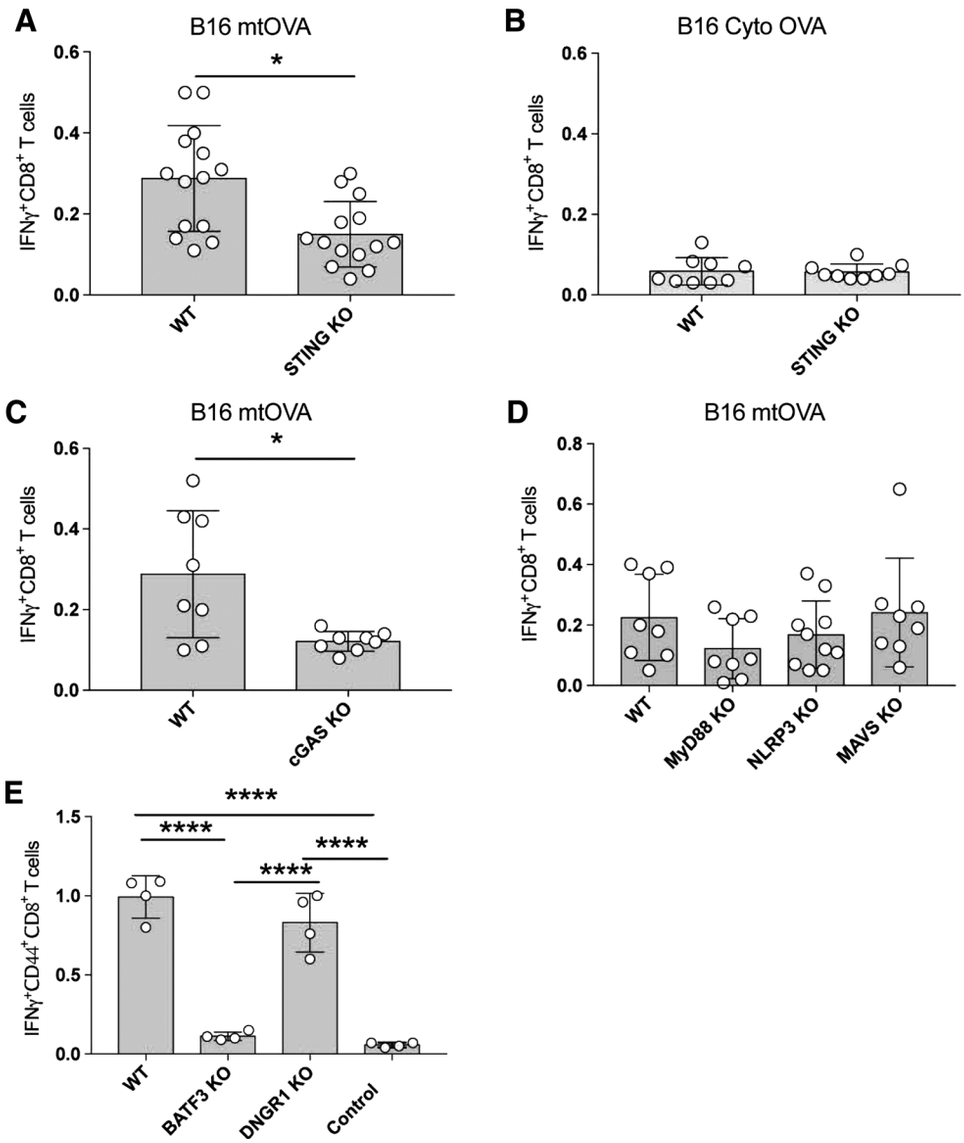

Figure 4.

Enhanced cross-priming of OVA-specific T cells is reduced in STING and cGAS knockout mice. **A** and **B,** WT or STING C57BL/6 knockout mice ($n = 5$ per group) were injected with 1×10^6 B16 mtOVA (**A**) or with 1×10^6 B16 cytoOVA (**B**) cells. Seven days after the injection, splenocytes were restimulated *in vitro* with the $OVA_{257–264}$ peptide (SIINFEKL), and the production of IFNγ was assessed by intracellular staining. Data from two or three independent experiments ($n = 5$) are shown. **C,** WT or cGAS knockout C57BL/6 mice ($n = 8$ per group) were injected with 1×10^6 B16 mtOVA. Seven days after the injection, splenocytes were restimulated with the $OVA_{257–264}$ peptide (SIINFEKL), and the production of IFNγ was assessed by intracellular staining. **D,** WT, MyD88 knockout, NLRP3 knockout, or MAVS knockout C57BL6 mice were injected with 1×10^6 B16 mtOVA. Seven days after the injections, splenocytes were restimulated with the $OVA_{257–264}$ peptide (SIINFEKL), and the production of IFNγ was assessed by intracellular staining. Bars represent the mean frequencies ± SD of 8 mice from two independent experiments, Two-tailed Student *t* test was used for comparing values. *, $P < 0.05$. **E,** Groups of WT or Batf3 and DNGR-1 C57BL6 knockout mice ($n = 5$) were injected with B16 mtOVA s.c. in the flank (1×10^6 cells/mouse). As a control, WT mice were injected with B16 without OVA. On day 7, splenocytes were restimulated with $OVA_{257–264}$ peptide (SIINFEKL) for 5 hours, and then IFNγ-secreting cells were identified by intracellular staining. ****, $P < 0.0001$ (one-way ANOVA followed by Tukey posttest). Values are expressed as mean ± SD. KO, knockout.

observed B16 mtOVA elicited H-$2K^b$/SIINFEKL–specific $CD8^+$ T-cell responses comparable with those observed in WT mice (**Fig. 4E**; Supplementary Fig. S3C).

These results demonstrate that the cGAS–STING pathway contributes to the enhanced immunogenicity of B16 mtOVA cells. These findings also indicate that priming of H-$2K^b$/SIINFEKL–specific $CD8^+$ T cells by the syngeneic B16 mtOVA requires $BATF3^+$ DCs, but it is not reduced by the lack of DNGR-1, MARCO, and SRA receptors.

Vaccination of B6 mice with B16 mitochondria elicits protective $CD8^+$ T-cell responses

Because mitochondria express more than 1,200 proteins, some of which are known to be mutated from germline sequences (39), we next

Published OnlineFirst March 23, 2020; DOI: 10.1158/2326-6066.CIR-19-0467

assessed whether mitochondria purified from WT B16 cells (i.e., not expressing OVA) could prime B16-specific CD8$^+$ T-cell responses. Mitochondria were purified from B16 cells or from mouse adult fibroblasts (MAF) from C57BL/6 mice and were then injected SC into WT C57BL/6 mice. Purity of the mitochondrial preparation was assessed by Western blot, demonstrating an enrichment of the mitochondrial protein TOM20 and ATP-B (the mitochondrial inner membrane ATP synthase subunit) in the mitochondrial fraction, whereas cytosolic GAPDH was almost absent (Supplementary Fig. S6A and S6B). Vaccinated or mock-treated mice were then challenged s.c. with B16 tumor cells 12 days after vaccination. We observed that vaccination with B16-derived mitochondria, but not with C57BL/6 MAF-derived mitochondria, produced a response capable of controlling tumor growth (**Fig. 5A**; Supplementary Fig. S7A). This effect was tumor specific, as mice vaccinated with mitochondria isolated from B16 cells and then challenged with the syngeneic, but unrelated, Lewis lung carcinoma, failed to control Lewis lung carcinoma growth (**Fig. 5B**; Supplementary Fig. S7B). Depletion of CD8$^+$ T cells resulted in enhanced tumor growth, with no significant difference between mice vaccinated with B16 mitochondria and the control group, demonstrating a role for CD8$^+$ T cells in controlling tumor growth this model (**Fig. 5C**; Supplementary Fig. S7C).

To further demonstrate the ability of CD8$^+$ T cells from mitochondria vaccinated mice to recognize B16 cells *in vitro*, mice were vaccinated with purified B16 mitochondria or vehicle control and then challenged with B16 cells. Splenocytes from these mice were then cocultured with B16 cells overnight. Splenocytes from naïve mice served as the no-challenge control. These experiments demonstrated that the frequency of B16-specific CD8$^+$ T cells isolated from mice vaccinated with B16 mitochondria was significantly greater than B16-specific CD8$^+$ T cells isolated from the control groups (**Fig. 5D**).

In conclusion, these results indicate that B16-derived mitochondria are a source of tumor antigens capable of inducing protective CD8$^+$ T-cell responses *in vivo*.

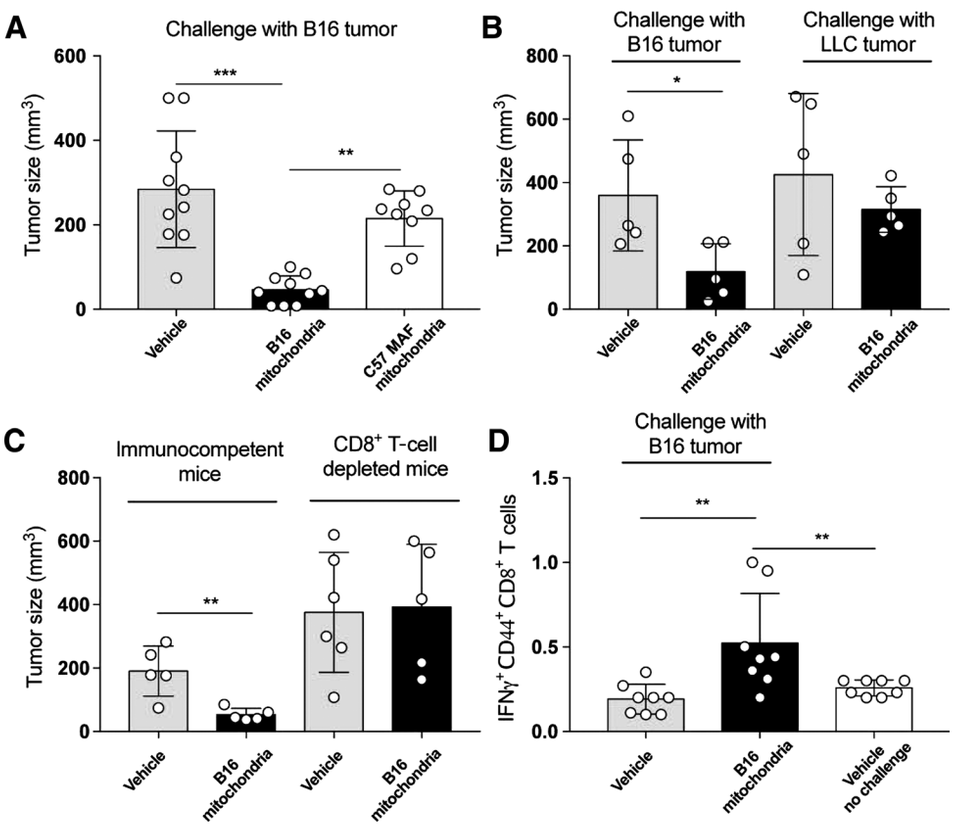

Figure 5.

Protective vaccination of naïve C57BL/6 mice with mitochondria purified from B16 tumors. **A,** Groups of mice ($n = 10$) were injected on day −12 with mitochondria isolated from B16 or from MAFs derived from C57BL/6 mice. On day 0, mice were injected s.c. with B16 cells (1.5×10^5 cells/mouse). Tumor measurements at day 14 are shown. Data are representative of two independent experiments with $n = 5$, and values are expressed as mean ± SD. ***, $P < 0.001$; **, $P < 0.01$ (one-way ANOVA followed by Tukey posttest). **B,** Groups of C57BL/6 mice were injected with mitochondria isolated from B16 cells on day −10. Ten days after injection (on day 0), mice were challenged with B16 cells or LLC (1.5×10^5 cells/mouse injected s.c.). Tumor measurements at day 14 are shown. Data are representative of two independent experiments with $n = 5$, and values are expressed as mean ± SD. Two-tailed Student *t* test was used for comparing values; *, $P < 0.05$. **C,** Groups of mice ($n = 5$–6) were injected on day −12 with mitochondria isolated from B16 cells or vehicle. On days −2, 0, and 5, mice were injected with an anti-CD8 antibody (clone 2.43) or an isotype control. On day 0, mice were injected s.c. with B16 tumor cells (1.5×10^5 cells/mouse). Tumor measurements at day 14 are shown. Data are representative of two independent experiments with $n = 5$, and values are expressed as mean ± SD. Two-tailed Student *t* test was used for comparing values. **, $P < 0.01$. **D,** Groups of mice ($n = 8$) were injected on day −12 with mitochondria isolated from B16 or with vehicle. On day 0, mice were injected s.c. with B16 tumor cell line (1.5×10^5 cells/mouse). On day 14, CD8$^+$ T cells were isolated from the spleen and cocultured with B16 cells, and the production of IFNγ was assessed by intracellular staining. Values are expressed as mean ± SD. ****, $P < 0.0001$; **, $P < 0.01$; *, $P < 0.05$ (one-way ANOVA followed by Tukey posttest).

Published OnlineFirst March 23, 2020; DOI: 10.1158/2326-6066.CIR-19-0467

CD8$^+$ T cells specific for mitochondrial-localized neoantigens in cancer patients

Finally, we extended our studies to humans by investigating the presence of CD8$^+$ T cells specific for mutated mitochondrial-localized proteins in human cancers. The frequencies of nonsynonymous somatic mutations in mitochondrial proteins that are expressed by genomic DNA from 9,508 samples across 31 cancer types from TCGA (version 02-04-2018) were investigated. We observed the presence of mutations of mitochondrial-localized proteins across different tumor types, with the highest average frequency present in endometrioid cancers (**Fig. 6A**). We therefore focused our studies on endometrial cancer patients and studied the immune response in 1 patient with a hypermutated phenotype caused by the loss of function of the proofreading DNA polymerase epsilon (POLE; ref. 25).

By comparing the sequences obtained from tumor and germline DNA, tumor-specific, nonsynonymous single-nucleotide variations were identified. RNA-sequencing was also performed to check the expression of potential neoepitopes (Supplementary file S1). A pipeline was used to predict mutant peptide binding affinity to the patient's HLA allele HLA-A*02:01. Epitopes were then prioritized based on their mitochondrial or nonmitochondrial localization, and 60 peptides were synthesized for each location group. The patient's PBMCs were stimulated and expanded in the presence of each peptide, and HLA-A2 tetramers loaded with mitochondrial or not mitochondrial-derived peptides were used to assess the presence of neoantigen-specific T cells in the expanded PBMC. We identified CD8$^+$ T cells recognizing 4 neoantigens derived from 2 mitochondrial-localized mutated proteins and 3 neoantigens derived from proteins localized in the cytosol (**Fig. 6B**; Supplementary Fig. S8), which were capable of specifically killing peptide-pulsed autologous EBV-LCLs (**Fig. 6C**) and producing IFNγ (**Fig. 6D**).

Discussion

Clinical results have demonstrated a significant correlation between the number of predicted HLA-binding peptides derived from mutated proteins in tumor cells and the efficacy of immune-checkpoint blocking antibody treatment in cancer patients (1). Thus, our ability to improve the identification and ranking of immunogenic neoantigens is needed to optimize the development of cancer vaccines and the effectiveness of checkpoint blockade therapies. Although several strategies are currently pursued to improve algorithms predicting immunogenicity of neoantigens (40, 41), further improvements are still required.

The results of our studies highlight the utility of considering the location of antigenic proteins in mitochondria as an additional criterion to prioritize neoantigen predictions, as we showed an increased immunogenicity of mitochondrial-localized OVA and NY-ESO-1 proteins. We demonstrated that their enhanced immunogenicity is due to their increased stability and to the activation of the cGAS/STING pathway. In contrast, cytosolic localized OVA and NY-ESO-1 proteins, which are rapidly degraded by the proteasome and efficiently directly presented by tumor cells *in vitro*, fail to induce strong antigen-specific CD8$^+$ T-cell responses *in vivo*. These results are supported by previously published papers demonstrating a correlation between protein stability and their cross-priming abilities (13, 32, 38). The more efficient cross-priming of mitochondrial-localized proteins is likely due to the efficient uptake of mitochondria by cross-priming CD103$^+$ DCs, compared with cytosolic OVA, and by a combination of the higher steady-state amount and enhanced DC maturation, possibly due to mitochondrial DNA.

The rate at which antigenic proteins are degraded in cross-presenting DC is also a determining factor in controlling the immunogenicity of cross-presented antigens (37, 42), which can be modulated by several factors, including the rate at which antigenic proteins exit from the endosomes/lysosomes to the cytosol in cross-presenting DCs (43), the expression of lysosomal proteases (44, 45), and the pH within lysosomes (44, 46, 47), which is shown to be higher in the lysosomes of DCs and improves cross-presentation of antigenic proteins (48). We found that the two forms of stable OVA (i.e., mod cytoOVA and mtOVA), which were localized in different compartments of B16 cells, displayed different abilities to prime the $OVA_{257-264}$–specific T-cell response. Although further experiments are warranted to dissect the mechanisms controlling these results, it is tempting to speculate that the observed differential priming abilities of B16 mod cytoOVA and B16 mtOVA cells may reflect differences in their processing events in cross-presenting DCs.

Different recognition pathways have been shown to provide the relevant signals for CD8$^+$ T-cell priming, including extracellular uric acid generated during cell death, which may stimulate an inflammatory response, mediated by NLRP3 inflammasome activation (49). Although we did not observe any difference between WT mice and NLRP3-deficient mice, we showed that lack of the STING/cGAS pathway significantly reduced priming of CD8$^+$ T cells specific for mitochondrial-localized proteins (34, 35). In contrast, DNGR-1, which was previously shown to be involved in the cross-presentation of cell-associated antigens (37), appeared not to be involved in the cross-presentation of mitochondrial OVA. Previous papers have provided insights into the mechanisms by which mitochondrial-derived proteins may intersect the antigen processing and presentation pathway (15, 16). However, these papers fail to demonstrate whether mitochondrial antigenic proteins can be efficiently taken up by DCs *in vivo* and cross-presented to antigen-specific CD8$^+$ T cells.

We have extended results obtained with model antigens (i.e., OVA and NY-ESO-1), by using endogenous B16 mitochondria as a source of specific mitochondrial antigens (39) and demonstrated their ability to induce B16-specific CD8$^+$ T-cell responses capable of controlling B16 growth *in vivo*. These results extend our previous findings obtained with mitochondrial-localized OVA and NY-ESO-1 protein by highlighting the strong immunogenicity of endogenous mitochondrial-localized antigenic proteins. In our analysis of CD8$^+$ T cells from an endometrial cancer patient, we identified an equal number of T-cell clones specific for either mitochondrial or nonmitochondrial neoantigens. However, we note that the expansion potential of the CD8$^+$ T cells that are specific for mitochondrial-localized epitopes is higher. This is consistent with the concept that tumor mitochondrial-localized neoantigens are able to prime a better CD8$^+$ T-cell response during tumor development.

Although cross-presentation events of epitopes derived from mitochondrial-localized proteins are involved in inducing strong priming of tumor-specific T cells, such response would not be sufficient to control tumor growth *in vivo*, unless the tumor cells are able to directly present epitopes derived from mitochondrial-localized proteins. Our results demonstrated that mtOVA B16 cells can directly present the OVA SIINFEKL epitope *in vivo*, albeit less efficiently than B16 cytoOVA cells, and that the combination of the higher frequency of OVA-specific T cells and their ability to recognize B16 mtOVA cells *in vivo* accounted for the greater control of tumor growth, compared with cytoOVA B16 cells. It has been previously shown that direct presentation of epitopes derived from mitochondrial proteins relies on

Published OnlineFirst March 23, 2020; DOI: 10.1158/2326-6066.CIR-19-0467

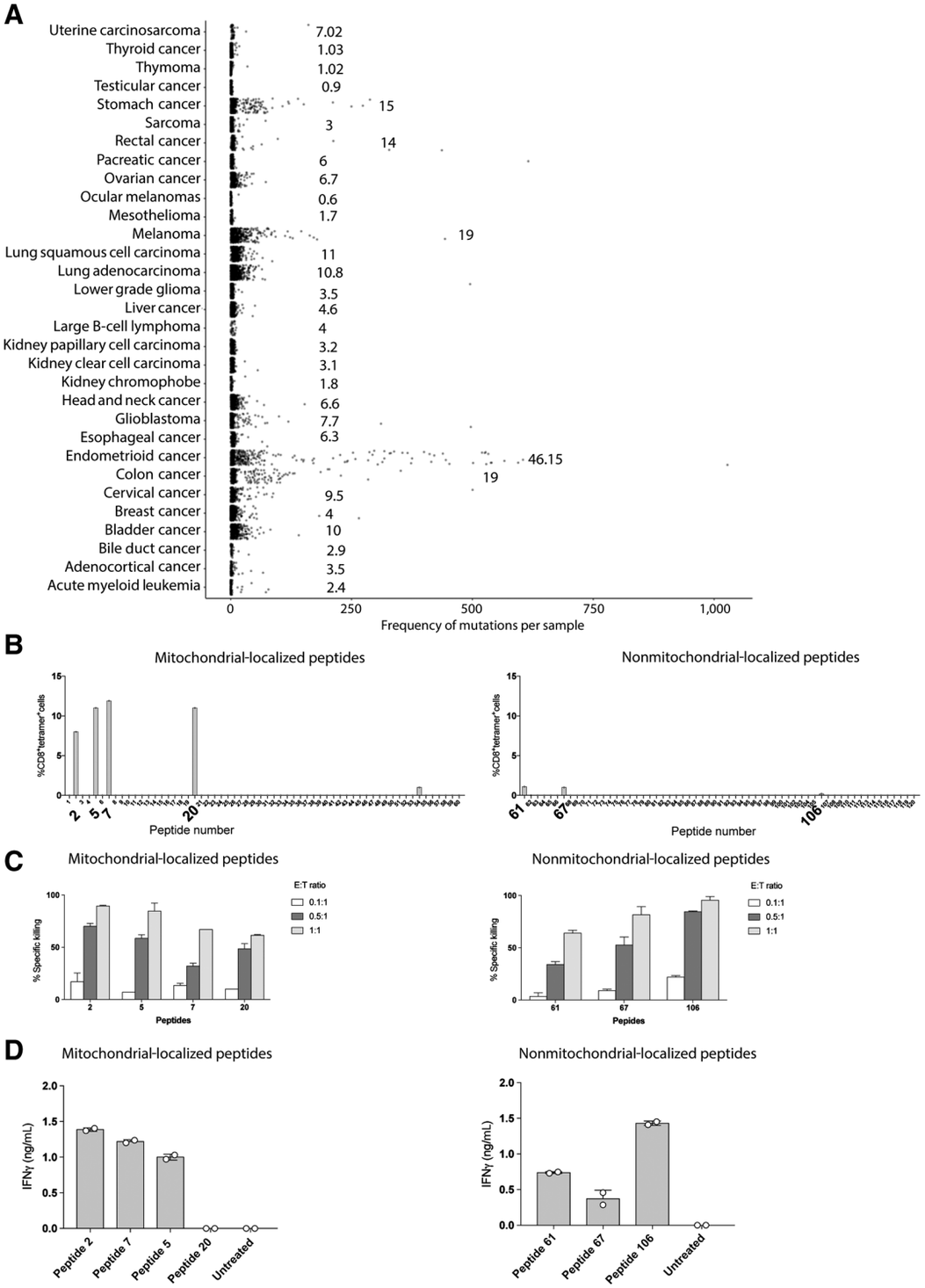

Figure 6.

Identification of CD8$^+$ T-cell clones specific for mitochondrial proteins in a cancer patient. **A,** Scatter plot shows the disperse frequencies of nonsynonymous somatic mutations in mitochondrial proteins in different cancer types; the average mutation number per cancer is reported. **B,** After restimulation, clones specific for mitochondrial-localized (left) and nonmitochondrial-localized proteins (right) were identified using MHC-I tetramers pulsed with the respective mutated peptide. The ability of identified CD8$^+$ T-cell clones to kill peptide-pulsed autologous EBV-immortalized B-cell lines (**C**) and to produce IFNγ was investigated (**D**). E:T ratio, effector-to-target ratio.

Published OnlineFirst March 23, 2020; DOI: 10.1158/2326-6066.CIR-19-0467

the generation and trafficking of mitochondrial-derived vesicles induced by heat shock, but not by IFNγ stimulation (15). We demonstrated that in order to detect the H-2K^b/SIINFEKL complex on the surface of B16 mtOVA and cytoOVA cells *in vitro*, B16 cells needed to be treated with IFNγ and TNFα. H-2K^b/SIINFEKL complexes were detectable *ex vivo* by flow cytometry on the surface of B16 mtOVA cells, suggesting that the inflammatory tumor microenvironment induces upregulation of SIINFEKL/H-2 K^b complexes. Indeed, we observed that upon depletion of CD8$^+$ T cells, B16 mtOVA cells lack surface expression of H-2K^b/SIINFEKL complexes, suggesting that cytokine expression by infiltrated tumor-specific CD8$^+$ T cells may be required to induce direct presentation of the SIINFEKL OVA epitope to detectable amounts.

In conclusion, our results demonstrate that the location of antigenic proteins in mitochondria significantly enhanced their ability to elicit a high frequency of antigen-specific CD8$^+$ T-cell responses *in vivo*. Such enhanced immunogenicity is controlled by cross-priming dependent events, which are facilitated by the steady-state amount of mitochondrial-localized proteins and by the activation of the STING–cGAS pathway. Our data showed a greater immunogenicity of mitochondrial-localized, mutated proteins during tumor development; boosting this preexisting immune response through personalized vaccination would be a novel strategy to enhance the efficacy of cancer immunotherapy treatments.

Disclosure of Potential Conflicts of Interest

No potential conflicts of interest were disclosed.

Authors' Contributions

Conception and design: G. Prota, U. Gileadi, A.V. Lechuga-Vieco, J.A. Enríquez, V. Cerundolo

Development of methodology: G. Prota, U. Gileadi, A.V. Lechuga-Vieco, J.-L. Chen, T.N. Schumacher

Acquisition of data (provided animals, acquired and managed patients, provided facilities, etc.): G. Prota, U. Gileadi, M. Rei, S. Galiani, M. Bedard, V.W.C. Lau, M. Artibani, S. Gordon, J. Rehwinkel, A.A. Ahmed, V. Cerundolo

Analysis and interpretation of data (e.g., statistical analysis, biostatistics, computational analysis): G. Prota, U. Gileadi, M. Rei, A.V. Lechuga-Vieco, S. Galiani, L.F. Fanchi, Z. Hu, J.A. Enríquez, A.A. Ahmed

Writing, review, and/or revision of the manuscript: G. Prota, U. Gileadi, M. Rei, A.V. Lechuga-Vieco, S. Gordon, J. Rehwinkel, J.A. Enríquez, A.A. Ahmed, V. Cerundolo

Administrative, technical, or material support (i.e., reporting or organizing data, constructing databases): G. Prota, J.-L. Chen

Study supervision: G. Prota, A.A. Ahmed, V. Cerundolo

Acknowledgments

This work was funded by the U.K. Medical Research Council, the Oxford Biomedical Research Centre, and Cancer Research UK (program grant C399/A2291). J.A. Enríquez was funded through MINECO (SAF2015-65633-R and SAF2015-71521-REDC). The Centro Nacional de Investigaciones Cardiovasculares Carlos III (CNIC) is supported by MINECO and the Pro-CNIC Foundation and is a SO-MINECO recipient (award SEV-2015-0505). A.A. Ahmed is supported by Ovarian Cancer Action, and Oxford Biomedical Research Centre, National Institute of Health Research. J. Rehwinkel acknowledges funding from the Wellcome Trust (grant number 100954). A.V. Lechuga-Vieco was supported by a Postdoctoral Fellowship from the Fundacion Alfonso Martin Escudero (Spain). The authors thank Oliver Schulz, Neil Rogers, and Caetano Reis e Sousa for providing DNGR-1 knockout and BATF3 knockout mice. The authors thank Kevin Maloy for providing MyD88 knockout mice. The authors thank Mariolina Salio and Giorgio Napolitani (University of Oxford) for critical revision of this article.

The costs of publication of this article were defrayed in part by the payment of page charges. This article must therefore be hereby marked *advertisement* in accordance with 18 U.S.C. Section 1734 solely to indicate this fact.

Received June 22, 2019; revised November 5, 2019; accepted March 12, 2020; published first March 23, 2020.

References

1. Yarchoan M, Hopkins A, Jaffee EM. Tumor mutational burden and response rate to PD-1 inhibition. N Engl J Med 2017;377:2500–1.
2. Schumacher TN, Schreiber RD. Neoantigens in cancer immunotherapy. Science 2015;348:69–74.
3. The problem with neoantigen prediction [editorial]. Nat Biotechnol 2017;35:97.
4. Vitiello A, Zanetti M. Neoantigen prediction and the need for validation. Nat Biotechnol 2017;35:815–7.
5. Lee CH, Yelensky R, Jooss K, Chan TA. Update on tumor neoantigens and their utility: why it is good to be different. Trends Immunol 2018;39:536–48.
6. Bjerregaard AM, Nielsen M, Hadrup SR, Szallasi Z, Eklund AC. MuPeXI: prediction of neo-epitopes from tumor sequencing data. Cancer Immunol Immunother 2017;66:1123–30.
7. Zhou Z, Lyu X, Wu J, Yang X, Wu S, Zhou J, et al. TSNAD: an integrated software for cancer somatic mutation and tumour-specific neoantigen detection. R Soc Open Sci 2017;4:170050.
8. Kim S, Kim HS, Kim E, Lee MG, Shin EC, Paik S, et al. Neopepsee: accurate genome-level prediction of neoantigens by harnessing sequence and amino acid immunogenicity information. Ann Oncol 2018;29:1030–6.
9. Roberts EW, Broz ML, Binnewies M, Headley MB, Nelson AE, Wolf DM, et al. Critical role for CD103(+)/CD141(+) dendritic cells bearing CCR7 for tumor antigen trafficking and priming of T cell immunity in melanoma. Cancer Cell 2016;30:324–36.
10. Cruz FM, Colbert JD, Merino E, Kriegsman BA, Rock KL. The biology and underlying mechanisms of cross-presentation of exogenous antigens on MHC-I molecules. Annu Rev Immunol 2017;35:149–76.
11. Headley MB, Bins A, Nip A, Roberts EW, Looney MR, Gerard A, et al. Visualization of immediate immune responses to pioneer metastatic cells in the lung. Nature 2016;531:513–7.
12. Xu MM, Pu Y, Han D, Shi Y, Cao X, Liang H, et al. Dendritic cells but not macrophages sense tumor mitochondrial DNA for cross-priming through signal regulatory protein alpha signaling. Immunity 2017;47:363–73.
13. Shen L, Rock KL. Cellular protein is the source of cross-priming antigen in vivo. Proc Natl Acad Sci U S A 2004;101:3035–40.
14. Rimoldi D, Muehlethaler K, Salvi S, Valmori D, Romero P, Cerottini JC, et al. Subcellular localization of the melanoma-associated protein Melan-AMART-1 influences the processing of its HLA-A2-restricted epitope. J Biol Chem 2001;276:43189–96.
15. Matheoud D, Sugiura A, Bellemare-Pelletier A, Laplante A, Rondeau C, Chemali M, et al. Parkinson's disease-related proteins PINK1 and parkin repress mitochondrial antigen presentation. Cell 2016;166:314–27.
16. Yamazaki H, Tanaka M, Nagoya M, Fujimaki H, Sato K, Yago T, et al. Epitope selection in major histocompatibility complex class I-mediated pathway is affected by the intracellular localization of an antigen. Eur J Immunol 1997;27:347–53.
17. Jin L, Hill KK, Filak H, Mogan J, Knowles H, Zhang B, et al. MPYS is required for IFN response factor 3 activation and type I IFN production in the response of cultured phagocytes to bacterial second messengers cyclic-di-AMP and cyclic-di-GMP. J Immunol 2011;187:2595–601.
18. Bridgeman A, Maelfait J, Davenne T, Partridge T, Peng Y, Mayer A, et al. Viruses transfer the antiviral second messenger cGAMP between cells. Science 2015;349:1228–32.
19. Michallet MC, Meylan E, Ermolaeva MA, Vazquez J, Rebsamen M, Curran J, et al. TRADD protein is an essential component of the RIG-like helicase antiviral pathway. Immunity 2008;28:651–61.
20. Choi EM, Chen JL, Wooldridge L, Salio M, Lissina A, Lissin N, et al. High avidity antigen-specific CTL identified by CD8-independent tetramer staining. J Immunol 2003;171:5116–23.

21. Denkberg G, Stronge VS, Zahavi E, Pittoni P, Oren R, Shepherd D, et al. Phage display-derived recombinant antibodies with TCR-like specificity against alpha-galactosylceramide and its analogues in complex with human CD1d molecules. Eur J Immunol 2008;38:829–40.
22. Porgador A, Yewdell JW, Deng Y, Bennink JR, Germain RN. Localization, quantitation, and in situ detection of specific peptide-MHC class I complexes using a monoclonal antibody. Immunity 1997;6:715–26.
23. Fernandez-Vizarra E, Ferrín G, Pérez-Martos A, Fernández-Silva P, Zeviani M, Enríquez JA. Isolation of mitochondria for biogenetical studies: an update. Mitochondrion 2010;10:253–62.
24. Cibulskis K, Lawrence MS, Carter SL, Sivachenko A, Jaffe D, Sougnez C, et al. Sensitive detection of somatic point mutations in impure and heterogeneous cancer samples. Nat Biotechnol 2013;31:213–9.
25. Temko D, Van Gool IC, Rayner E, Glaire M, Makino S, Brown M, et al. Somatic POLE exonuclease domain mutations are early events in sporadic endometrial and colorectal carcinogenesis, determining driver mutational landscape, clonal neoantigen burden and immune response. J Pathol 2018;245:283–96.
26. Stronen E, Toebes M, Kelderman S, van Buuren MM, Yang W, van Rooij N, et al. Targeting of cancer neoantigens with donor-derived T cell receptor repertoires. Science 2016;352:1337–41.
27. Chen JL, Dawoodji A, Tarlton A, Gnjatic S, Tajar A, Karydis I, et al. NY-ESO-1 specific antibody and cellular responses in melanoma patients primed with NY-ESO-1 protein in ISCOMATRIX and boosted with recombinant NY-ESO-1 fowlpox virus. Int J Cancer 2015;136:E590–601.
28. Rodenko B, Toebes M, Hadrup SR, van Esch WJ, Molenaar AM, Schumacher TN, et al. Generation of peptide-MHC class I complexes through UV-mediated ligand exchange. Nat Protoc 2006;1:1120–32.
29. Palmowski MJ, Lopes L, Ikeda Y, Salio M, Cerundolo V, Collins MK. Intravenous injection of a lentiviral vector encoding NY-ESO-1 induces an effective CTL response. J Immunol 2004;172:1582–7.
30. Norbury CC, Basta S, Donohue KB, Tscharke DC, Princiotta MF, Berglund P, et al. CD8+ T cell cross-priming via transfer of proteasome substrates. Science 2004;304:1318–21.
31. Basta S, Stoessel R, Basler M, van den Broek M, Groettrup M. Cross-presentation of the long-lived lymphocytic choriomeningitis virus nucleoprotein does not require neosynthesis and is enhanced via heat shock proteins. J Immunol 2005; 175:796–805.
32. Townsend A, Bastin J, Gould K, Brownlee G, Andrew M, Coupar B, et al. Defective presentation to class I-restricted cytotoxic T lymphocytes in vaccinia-infected cells is overcome by enhanced degradation of antigen. J Exp Med 1988; 168:1211–24.
33. Yewdell JW, Schubert U, Bennink JR. At the crossroads of cell biology and immunology: DRiPs and other sources of peptide ligands for MHC class I molecules. J Cell Sci 2001;114:845–51.
34. Woo SR, Fuertes MB, Corrales L, Spranger S, Furdyna MJ, Leung MY, et al. STING-dependent cytosolic DNA sensing mediates innate immune recognition of immunogenic tumors. Immunity 2014;41:830–42.
35. Deng L, Liang H, Xu M, Yang X, Burnette B, Arina A, et al. STING-dependent cytosolic DNA sensing promotes radiation-induced type I interferon-dependent antitumor immunity in immunogenic tumors. Immunity 2014; 41:843–52.
36. Hildner K, Edelson BT, Purtha WE, Diamond M, Matsushita H, Kohyama M, et al. Batf3 deficiency reveals a critical role for CD8alpha^{+} dendritic cells in cytotoxic T cell immunity. Science 2008;322:1097–100.
37. Sancho D, Joffre OP, Keller AM, Rogers NC, Martínez D, Hernanz-Falcón P, et al. Identification of a dendritic cell receptor that couples sensing of necrosis to immunity. Nature 2009;458:899–903.
38. Guo C, Yi H, Yu X, Hu F, Zuo D, Subjeck JR, et al. Absence of scavenger receptor A promotes dendritic cell-mediated cross-presentation of cell-associated antigen and antitumor immune response. Immunol Cell Biol 2012;90:101–8.
39. Lower M, Renard BY, de Graaf J, Wagner M, Paret C, Kneip C, et al. Confidence-based somatic mutation evaluation and prioritization. PLoS Comput Biol 2012;8: e1002714.
40. Balachandran VP, èuksza M, Zhao JN, Makarov V, Moral JA, Remark R, et al. Identification of unique neoantigen qualities in long-term survivors of pancreatic cancer. Nature 2017;551:512–6.
41. Luksza M, Riaz N, Makarov V, Balachandran VP, Hellmann MD, Solovyov A, et al. A neoantigen fitness model predicts tumour response to checkpoint blockade immunotherapy. Nature 2017;551:517–20.
42. Chatterjee B, Smed-Sörensen A, Cohn L, Chalouni C, Vandlen R, Lee BC, et al. Internalization and endosomal degradation of receptor-bound antigens regulate the efficiency of cross presentation by human dendritic cells. Blood 2012;120: 2011–20.
43. Gros M, Amigorena S. Regulation of antigen export to the cytosol during cross-presentation. Front Immunol 2019;10:41.
44. Delamarre L, Pack M, Chang H, Mellman I, Trombetta ES. Differential lysosomal proteolysis in antigen-presenting cells determines antigen fate. Science 2005;307: 1630–4.
45. Lennon-Dumenil AM, Bakker AH, Maehr R, Fiebiger E, Overkleeft HS, Rosemblatt M, et al. Analysis of protease activity in live antigen-presenting cells shows regulation of the phagosomal proteolytic contents during dendritic cell activation. J Exp Med 2002;196:529–40.
46. Savina A, Jancic C, Hugues S, Guermonprez P, Vargas P, Moura IC, et al. NOX2 controls phagosomal pH to regulate antigen processing during crosspresentation by dendritic cells. Cell 2006;126:205–18.
47. Mantegazza AR, Savina A, Vermeulen M, Pérez L, Geffner J, Hermine O, et al. NADPH oxidase controls phagosomal pH and antigen cross-presentation in human dendritic cells. Blood 2008;112:4712–22.
48. Accapezzato D, Visco V, Francavilla V, Molette C, Donato T, Paroli M, et al. Chloroquine enhances human CD8+ T cell responses against soluble antigens in vivo. J Exp Med 2005;202:817–28.
49. Shi Y, Evans JE, Rock KL. Molecular identification of a danger signal that alerts the immune system to dying cells. Nature 2003;425:516–21.

Published OnlineFirst March 23, 2020; DOI: 10.1158/2326-6066.CIR-19-0467

Cancer Immunology Research

Enhanced Immunogenicity of Mitochondrial-Localized Proteins in Cancer Cells

Gennaro Prota, Uzi Gileadi, Margarida Rei, et al.

Cancer Immunol Res 2020;8:685-697. Published OnlineFirst March 23, 2020.